



1 **Fill dynamics and sample mixing in the AirCore**

2 **Pieter P. Tans**

3 **Global Monitoring Laboratory, National Oceanic and Atmospheric Administration**

4 **325 Broadway, Boulder, CO 80305**

5

6 **Abstract**

7 The AirCore is a long coiled tube that acts as a “tape recorder” of the composition of air as it is  
8 slowly filled or flushed. When launched by balloon with one end of the tube open and the other  
9 closed, the initial fill air flows out during ascent as the outside air pressure drops. During descent  
10 atmospheric air flows back in. We describe how we can associate the position of an air parcel in  
11 the tube with the altitude it came from by modeling the dynamics of the fill process. The  
12 conditions that need to be satisfied for the model to be accurate are derived. The extent of mixing  
13 of air parcels that enter at different times is calculated, so that we know how many independent  
14 samples are in the tube upon landing, and later when the AirCore is analyzed.

15

16 **1 Introduction**

17 When the Aircore is filling with atmospheric air coming in through the open end the newly  
18 sampled air pushes the air that is already in the tube deeper into the tube while compressing it.  
19 This mode of sampling is entirely passive, relying on the pressure continuing to increase as the  
20 altitude becomes lower during descent. The AirCore could also be flushed by a pump without  
21 any need for pressure changes of the outside air that is being sampled. I conceived the idea of  
22 AirCore in the late 1990s after we had found ~100 year old air, as indicated by the measured  
23 levels of CO<sub>2</sub> and CH<sub>4</sub>, near the bottom of the firn layer at a depth of ~90 m at the South Pole  
24 (Battle, 1996). The air was very old despite the fact that there was still open contact with the  
25 present-day atmosphere. Over distances of tens of meters or more molecular diffusion is  
26 exceedingly slow! The root-mean-square (rms) molecular diffusion distance is  $X_{rms} = (2Dt)^{0.5}$ .  $D$   
27 is diffusivity in air, for CO<sub>2</sub> it is 0.140 cm<sup>2</sup> s<sup>-1</sup> at 1 bar and 0 degree C,  $t$  is time in seconds. After  
28 one year the rms diffusion distance for CO<sub>2</sub> in air would be ~30 m which would be the scale of  
29 spreading if there is no macroscopic air motion at all. In addition, diffusivity deep in the firn is  
30 significantly slower than in open air because the air path from the bottom of the firn to the  
31 atmosphere has many detours going through the pores that are still open.

32 In collaboration with Jim Smith and Michael Hahn, we verified that there is very little mixing  
33 along the length of the tube by pushing slugs of air from two different reference air cylinders,  
34 alternating between high and low CO<sub>2</sub>, through a long coiled tube. We also stored air for several



35 hours before analysis. It all looked good. Then we tried a balloon flight. In order to make the  
36 payload lighter we switched from stainless steel to aluminum tubing, because of our excellent  
37 experience with long term gas storage in high pressure aluminum cylinders. It did not work at all.  
38 The easily bendable tube was made of a soft aluminum alloy, very different from the high  
39 pressure cylinders. We found that the tube made CO<sub>2</sub> disappear very effectively. It was going to  
40 take more effort to make it successful, and we did not have much time to devote to it. So the  
41 project languished for several years until Anna Karion, Colm Sweeney, and Tim Newberger  
42 were able to pick it up again. At the urging of Sandy MacDonald, who was director of NOAA's  
43 Earth System Research Laboratory at the time, I applied for a patent in August 2006. He pointed  
44 out that there are people trolling the scientific literature, conference proceedings, etc. to find  
45 ideas that could be patented, so that we might find ourselves having to pay somebody else to use  
46 our own idea. Instead, we wanted the AirCore to be freely useable (and improved) by everyone,  
47 so that my patent (Tans, 2009) was intended to be a defensive action!

48 We realized that AirCore technology could become extremely useful for the validation of  
49 satellite retrievals of column-averaged mole fractions of greenhouse gases. The measurements of  
50 a gas sample captured by the AirCore are calibrated, but care has to be taken, as with all air  
51 samples in containers, that no artefacts are introduced by the container or by gas handling  
52 procedures. In contrast, remote sensing estimates of greenhouse gases can in principle never be  
53 calibrated. Metrology, the science of measurement, defines what a calibration is. Using a  
54 measurement standard, one presents the measurement method with a known value, under  
55 controlled conditions, so that the measurement indication is related to a quantity value  
56 (paraphrased from VIM3, JCGM 200:2008). In the case of greenhouse gases in the atmosphere  
57 the conditions cannot be controlled. In addition, we realized that the regular deployment of  
58 AirCores could be a cost effective way to monitor and study an evolving atmospheric circulation  
59 as climate change progresses, as proposed by Fred Moore (2014).

60

## 61 **2. The physical principle that makes the AirCore work – molecular diffusion**

62 Diffusive mixing over large distances is exceedingly slow, but there is another use of diffusion.  
63 Flow inside the tube is laminar, which has maximum speed in the center and zero speed at the  
64 wall. With velocities that differ from zero to some finite value, why does laminar flow **not**  
65 “smear out” our tape recorder signal by mixing air parcels that came in at different times? Again,  
66 molecular diffusion comes to the rescue. Using the square root relationship above, if the inner  
67 radius of the tube is 0.3 cm, it takes a CO<sub>2</sub> molecule on average only 0.03 s (at 1 bar pressure) to  
68 diffuse from the wall to the radius where the velocity equals the average velocity inside the tube.  
69 Any molecule will be close to the wall, as well as near the center, of the tube many times per  
70 second. Therefore the speed of all molecules in the long direction of the tube, averaged over a  
71 few seconds, is very nearly the same. However, the AirCore idea does not work so well for  
72 liquids. In water the molecular diffusivity is ~10,000 times lower than in air at 1 bar, so that the



73 smearing of a tape recorder signal could be very large. To compensate for such low diffusivity  
74 both the diameter of the tube and the flow speed will have to be kept low, and there will also be  
75 capillary effects.

76 The AirCore collects a continuous sample. Instead of valves, distance in the tube is used to keep  
77 separated the air that has been sampled from different pressure altitudes. The number of  
78 independent samples (the inverse of vertical resolution) in the tube decreases as the time between  
79 collection and measurement becomes longer. The measurement, or “read-out” of the vertical  
80 profile, is carried out by attaching an analytical instrument to one end of the tube and a cylinder  
81 with air of well-known composition to the other end. The latter pushes the sampled air slowly  
82 through the analyzer. The procedure, as well as various tests of mixing, has been described by  
83 Karion (2010).

84

### 85 3. Dynamics of the fill process

86 How do we accurately associate position in the tube with the geometric altitude or pressure  
87 altitude that the sample at that position came from? It is the first question we address in this  
88 paper. The filling does not occur uniformly as a function of pressure altitude. The second  
89 question is how far the mixing of adjacent air parcels extends as a result of molecular diffusion,  
90 and secondarily as a result of the flow itself. I wrote the first version of the algorithm to make the  
91 association of altitude with position in 2005, called `rocketfall.pro`, coded in Interactive Data  
92 Language (IDL). Undergraduate students in the engineering department at the University of  
93 Colorado were getting ready to put an AirCore on a NASA rocket, and we were worried about  
94 there not being enough time to passively collect air from the stratosphere as the rocket was  
95 falling at supersonic speeds. There have been several successive versions of the algorithm since  
96 then. The version of July 2021 is described here.

97 We use a fluid dynamics model and flight data, namely the pressure and temperature of outside  
98 air and the temperature of the tube as input data. The starting point is Poiseuille’s equation for  
99 steady state laminar flow in a tube with circular cross section:

$$100 \quad Q_m = \frac{-\rho \pi r^4}{8 \eta} \frac{dP}{dz}, \quad \text{or} \quad Q_n = \frac{-\rho_n \pi r^4}{8 \eta} \frac{dP}{dz} \quad \text{Eq. 1}$$

101 in which  $Q_m$  is mass flow ( $\text{kg s}^{-1}$ ),  $Q_n = Q_m/M$  is amount flow ( $\text{mol s}^{-1}$ ) with  $M$  molecular weight  
102 of dry air ( $0.02896 \text{ kg mol}^{-1}$ ),  $\rho$  is gas density ( $\text{kg m}^{-3}$ ),  $\rho_n$  is amount density ( $\rho/M$  in  $\text{mol m}^{-3}$ ),  $\eta$   
103 is viscosity ( $\text{kg m}^{-1} \text{ s}^{-1}$ ),  $r$  is tube radius (m),  $P$  is pressure in Pascal ( $\text{kg m}^{-1} \text{ s}^{-2}$ ), and  $z$  is  
104 distance along the tube (m). Pressure is given by the ideal gas law as  $P = (n/V) RT$ , with  $n/V = \rho_n$   
105 the number density in  $\text{mol m}^{-3}$ ,  $T$  is temperature in degrees Kelvin (K), and  $R$  the universal gas  
106 constant,  $8.3144 \text{ J mol}^{-1} \text{ K}^{-1}$ . The flow velocity is parabolic as a function of radius, zero at the  
107 wall, and maximum in the center where the speed is twice the average speed.



108 The viscosity ( $\eta$ ) depends on temperature, but it is very nearly independent of pressure in our  
109 range of interest. The latter is of primary importance to the fill process. A simple approximate  
110 molecular expression for viscosity is  $\eta \cong (1/3) \rho \bar{c} \lambda$ , in which  $\bar{c}$  is the average molecular speed  
111 and  $\lambda$  is the mean free path between collisions which is inversely proportional to  $\rho$  (Jeans, 1952).  
112 Since the volume flow ( $\text{m}^3 \text{s}^{-1}$ ) is  $Q_v = Q_m/\rho$ , Eq. 1 states that the volume flow depends on  
113 viscosity, but not on gas density. It takes the same amount of force (pressure difference) to push  
114 the same volume flow irrespective of the density of air in that volume. During steady flow  
115 through any tube the flow needs to speed up at the low pressure end to conserve mass so that the  
116 pressure gradient always steepens at the low pressure end.

117 The z-coordinate is for position along the length of the tube. The pressure change at any point in  
118 a small section of the tube with length  $dz$  can be due to temperature change or to more amount  
119 flow coming in from  $z$  than leaving from  $z+dz$ . The latter term is

$$\frac{d\rho_n}{dt} = -\frac{1}{\pi r^2} \frac{dQ_n}{dz}, \quad \text{so that}$$
$$\frac{dP}{dt} = \rho_n R \frac{dT}{dt} + RT \frac{d\rho_n}{dt} = \frac{P}{T} \frac{dT}{dt} - \frac{RT}{\pi r^2} \frac{dQ_n}{dz} \quad \text{Eq. 2}$$

122 If we assume that the tube is round (not elliptical for example) the amount flow  $Q_n$  is given by  
123 Poiseuille's equation, and Eq. (2) can be represented numerically in a very efficient manner. In  
124 that case the flow is in effect solved as a succession of steady state flows that evolve slowly in  
125 time and along the length of the tube. In the rest of this section we will discuss a number of  
126 assumptions we are making for our "succession of steady state flows" approximation to Eq. (2)  
127 to be satisfactory.

128 The first one is that inertial effects, i.e. accelerations, die out very rapidly. Suppose we suddenly  
129 set the pressure gradient that is driving the flow to zero. What is the time scale for the flow to die  
130 down? We can estimate the time it takes for the flow to adjust by using Eq. 1. The average speed  
131 of the flow is  $\mathbf{v}_{\text{avg}} = Q_v/(\pi r^2) = (r^2/8\eta) (\Delta P/\Delta z)$ . The momentum of the flow in length  $\Delta z$  is  $\mathbf{v}_{\text{avg}} \rho$   
132  $\pi r^2 \Delta z$  which equals  $Q_m \Delta z$  (neglecting the sign). The rate of change of momentum is given by  
133 the frictional force which is equal and opposite to the pressure force that was driving the flow in  
134 Eq. 1. The adjustment time scale of the flow is momentum divided by the frictional force,

$$\tau = \frac{Q_m \Delta z}{\Delta P \pi r^2} = \frac{\rho r^2}{8 \eta} \quad \text{Eq. 3}$$

136 For a tube with a radius of 3 mm and  $\rho$  corresponding to 1 bar and 285 K,  $\tau \cong 0.07$  s. At an  
137 altitude where the density is 10 times lower ( $\sim 18$  km),  $\tau \cong 0.007$  s. Recently NOAA GML has  
138 been flying AirCores with  $r \cong 1.46$  mm, for which the adjustment time at 1 bar and 285 K is  $\tau \cong$   
139 0.017 s. A succession of steady state flows is indeed a very close approximation.



140 Next we assume that the temperature of the gas is the same as that of the wall. How rapidly does  
141 the temperature of the gas equilibrate with the wall of the tube? The heat capacity of a volume of  
142 air is  $c_p \rho_n \cong (7/2) R * P/RT$  in which  $c_p$  is the molar heat capacity at constant pressure and  $\rho_n$  is  
143 the number density ( $\text{mol m}^{-3}$ ) of the gas, so that  $c_p \rho_n$  has units of  $\text{J m}^{-3} \text{K}^{-1}$ . The heat  
144 conductivity of gas is  $\kappa \cong (1/3) c_v \rho_n \mathbf{c} \lambda$  (Jeans, 1952) in which  $c_v$  is the molar heat capacity at  
145 constant volume,  $\mathbf{c}$  is the average speed of individual molecules and  $\lambda$  the mean free path. It has  
146 units of  $(\text{J/s}) \text{m}^{-2} (\text{K/m})^{-1}$ , the heat flow per area per temperature gradient. As in the previous  
147 paragraph we divide the heat energy change corresponding to  $\Delta T$  in a volume of gas residing in a  
148 length  $\Delta z$  by the heat flow from the wall assuming the temperature gradient is close to  
149  $(\Delta T)/(0.5r)$ . That gives

$$150 \quad \tau = \frac{c_p \rho_n \pi r^2 \Delta z \Delta T}{(1/3) c_v \rho_n \mathbf{c} \lambda 2\pi r \Delta z \Delta T / (0.5r)} = \frac{c_p}{c_v} \frac{3 r^2}{4 \mathbf{c} \lambda} \quad \text{Eq. 4}$$

151 which has units of seconds. For  $r = 3 \text{ mm}$  and  $\lambda$  corresponding to 1 bar, and 285 K, the  
152 adjustment time is  $\tau \cong 0.31 \text{ s}$ , and shorter at lower pressures. For  $r = 1.46 \text{ mm}$   $\tau \cong 0.07 \text{ s}$ .

153 Is the flow always laminar as Eq. 1 assumes? If Reynolds number,  $Re = (\rho \mathbf{v}_{\text{avg}} d)/\eta$ , in which  $d$  is  
154 the diameter of the tube, stays below 1000, the flow will remain laminar.  $Re$  is estimated from  
155 the calculated velocities,  $\rho/\eta$ , and tube dimensions for every flight. It is highest just before  
156 landing when it typically has a value of  $\sim 15$ .

157 The tube is wound up in a coil with typical diameter 20 to 30 cm. As the flow goes around the  
158 coil there will be a centrifugal force away from the center of the coil. The centrifugal force is  
159 greatest where the flow has the maximum velocity,  $2 \mathbf{v}_{\text{avg}}$ , very near the center of the tube. This  
160 sets up a secondary flow in the plane perpendicular to the main flow, outward in the center of the  
161 tube and back along the walls. The location of maximum velocity is also pushed outward a bit.  
162 This increases flow resistance leading to slightly lower  $Q_m$  for the same pressure gradient in the  
163 dimension  $z$  along the length of the tube. However, there are other subtle effects with the  
164 opposite sign that could facilitate the flow a little (Berg, 2004). Correction factors to flow in a  
165 straight tube have been calculated using Dean's number,  $De = Re (r/R)^{0.5}$ , in which  $Re$  is  
166 Reynolds number and  $R$  is the coil radius. NOAA GML has flown AirCores with  $r/R$  from 1/50  
167 to 1/70. Thus  $De$  is always smaller than 15  $(0.02)^{0.5} \cong 2$  during a flight. Berg et al. (2004)  
168 present data to estimate that the relative flow correction is smaller than  $+1 \cdot 10^{-5}$  for our  
169 parameters. If we were to wind our coil much tighter, say with  $r/R$  of 1/20, then the maximum  
170 relative flow correction during a flight would be  $+2 \cdot 10^{-4}$  for the same Reynolds number.  
171 Therefore we can neglect the corrections for the tube coil curvature.

172 If the tube is elliptical instead of circular, there is a good approximation for the change in flow  
173 resistance. Following Lekner (2019), Eq.1 can be written for volume flow as  $(\eta Q_v) / (dP/dz) =$   
174  $\pi r^4 / 8$ , neglecting the sign. Note that  $\pi r^4 / 8$  equals  $A^3 / (2 P^2)$  for a circular cross section, with  
175  $A$  the cross sectional area, and  $P$  the perimeter of the tube. Lekner shows that  $A^3 / (2 P^2)$  applies



176 quite generally for many cross sectional shapes. So if the tube is somewhat squashed into an  
177 ellipse with major axis 1.05 times the original radius, and a minor axis slightly smaller (in order  
178 to keep the perimeter the same) than 0.95 times radius, the term  $A^3 / (2 P^2)$  has become ~1%  
179 smaller. This is not a major effect.

180 We assumed the ideal gas law. Non-ideality is often described by the virial expansion relating  
181 pressure and density,  $PV/nRT = 1 + B(n/V) + C(n/V)^2 + \dots$ . Note that  $n/V$  is called  $\rho_n$  above.  
182 Taking only the second (and largest) virial coefficient  $B$  ( $\text{m}^3/\text{mol}$ ) into account we can  
183 approximate the number density  $\rho_n$  as  $(P/RT)(1 - BP/RT)$ . The relative change of number density  
184 is thus  $BP/RT$  which has dimension one. At 300 K and 1 bar,  $B$  is  $-7.3 \cdot 10^{-6} \text{ m}^3/\text{mol}$   
185 (Sevast'yanov, 1986) which leads to a relative density increase of  $2.9 \cdot 10^{-4}$ .  $B$  increases to  $-18.9$   
186  $\cdot 10^{-6}$  and  $-37.8 \cdot 10^{-6} \text{ m}^3/\text{mol}$  at 250 K and 200 K respectively, but at the higher altitudes the  
187 density is lower so that the largest non-ideality effect occurs near the ground. Therefore the  
188 fractional density increase relative to ideal gas during a flight remains well below 0.001

189 When the mean free path increases at lower pressures there could be “wall-slip”, non-zero  
190 velocity at the wall which can be modeled as an effective decrease in viscosity increasing the  
191 volume flow. Berg (2005) gives an approximate expression for the factor by which the flow  
192 increases,  $1 + 4 K_{\text{slip}} \text{Kn}$ , where  $K_{\text{slip}}$  is a number close to 1 which depends on intermolecular  
193 forces, and  $\text{Kn}$  is the Knudsen number,  $\lambda/d$ , with  $d$  being the internal diameter of the tube. At  
194 high altitude, say 10 millibar (mb),  $\lambda \sim 7 \cdot 10^{-4} \text{ cm}$ , so that  $\text{Kn} \sim 0.001$  for  $d = 0.6 \text{ cm}$ . For  $d = 0.3$   
195 cm the flow would be increased by a factor 1.009 at 10 mb.

196 When  $\text{Kn}$  becomes larger than  $\sim 0.01$  a transition region of pressure is entered in which the flow  
197 changes gradually from bulk flow of gases, laminar in our case, to molecular flow (O'Hanlon,  
198 1980). In the latter flow regime the gas sample enters the tube as individual molecules, and gases  
199 with higher molecular speed (lower mass) enter the tube more rapidly, so that the air sample may  
200 not represent the composition of outside air, whereas in bulk flow an overwhelming fraction of  
201 all molecules are equally swept along. As an example, for an AirCore with opening diameter of  
202 0.3 cm this flow transition starts at a pressure altitude of  $\sim 2 \text{ mb}$ . Therefore, approximately 43 km  
203 might be the highest altitude that can be sampled with this diameter opening without first  
204 quantitatively investigating molecular flow effects, although this limit depends also on the  
205 sampling accuracy we require.

206 The above expressions for viscosity,  $\eta \cong (1/3) \rho \mathbf{c} \lambda$ , and heat conductivity,  $\kappa \cong (1/3) c_v \rho_n \mathbf{c} \lambda$ ,  
207 and similar for diffusivity,  $D \cong (1/3) \mathbf{c} \lambda$  are approximate. More precise forms of these equations  
208 vary depending on the treatment of intermolecular forces. Instead, we use a curve fit to empirical  
209 data for viscosity in dry air as a function of temperature, as presented by Kadoya (1985). The  
210 empirical data show, as expected, that there is no dependence on pressure in our range of  
211 interest.

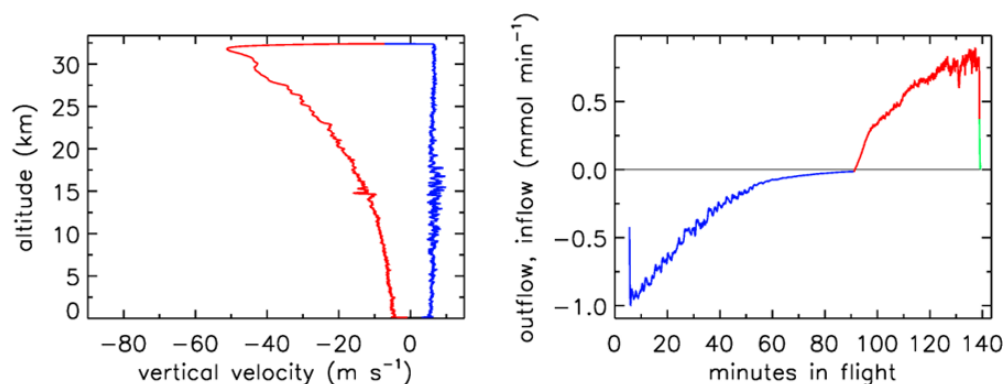


212 For diffusivity of trace gases in air as a function of temperature and pressure we use the  
213 empirical equation presented by Massman (1999),  $D(T,P) = D_0 (P_0/P) (T/T_0)^{1.81}$ .  $D_0$  is the  
214 diffusivity, different for each trace gas in air, at 1 atmosphere air pressure ( $P_0$ ) and 0 degrees  
215 centigrade ( $T_0$ ). This will be used when we calculate mixing of air samples entering the AirCore  
216 sequentially. Mixing is caused both by molecular diffusion ( $X_{rms} = (2Dt)^{0.5}$ , see above) and by  
217 the quadratic velocity profile of laminar flow, with zero speed at the wall and maximum speed in  
218 the center. The latter is called Taylor diffusion (Karion, 2010), and is given by a diffusivity  
219 constant  $D_T = v_{avg}^2 r^2 / (48 D)$  which has the same dimensions as  $D$ ,  $m^2 s^{-1}$ .

220

#### 221 4. Calculated in- and outflow results for some flights

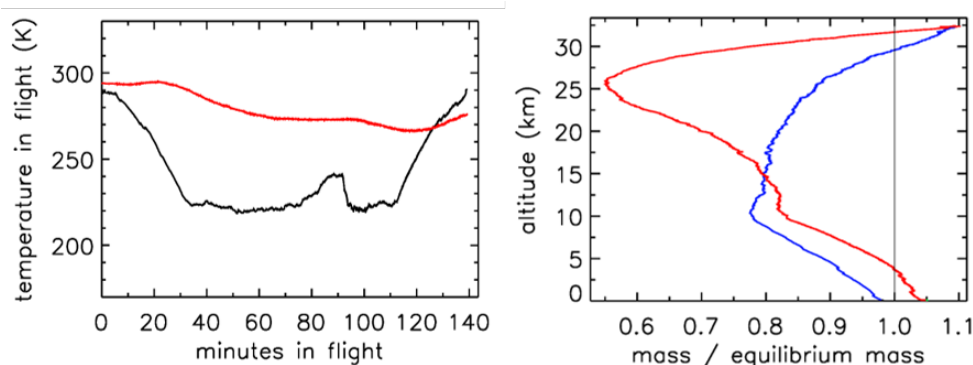
222 In Figures 1- 4 the flight is shown of a small diameter (1/8 inch, internal diameter 2.92 mm)  
223 AirCore (GMD008), with 93 m length and internal volume 619 cc, near Trainou, France (48.0  
224 °N, 2.1 °E) on 20 June 2019. The ascent velocity of the helium balloon is nearly constant, while  
225 the rate of mass outflow decreases steadily as a function of time as the pressure outside and  
226 inside the AirCore drops. The descent velocity with parachute accelerates nearly linearly in the



227

228 *Figure 1. Descent velocity (negative) and rate of fill air outflow followed by air sample inflow*  
229 *during flight of GMD008. Blue, ascent; red, descent; green, on the ground*

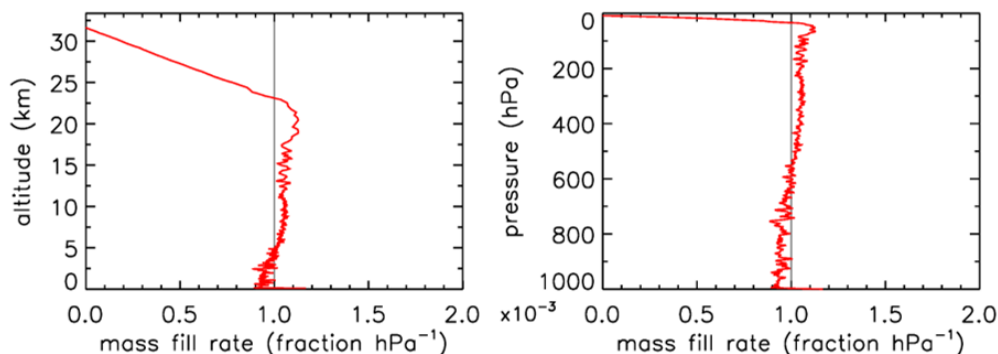
230 first 10 seconds to about 50 m s<sup>-1</sup> as the pressure at high altitudes is too low for air friction to  
231 slow it down enough. The initial descent can be a chaotic tumble until the parachute gets a  
232 “grip”. Outflow and inflow in the tube are calculated with the fill dynamics program described  
233 below in section 8.



234  
235 *Figure 2. Flight of GMD008. Left panel: Temperatures in degrees Kelvin. AirCore tube, red;*  
236 *outside air, black. Right panel: Blue, ascent; red, descent.*

237 In Figure 2 the outside air temperature first cools while in the troposphere, then becomes nearly  
238 constant in the tropopause, and starts increasing again higher into the stratosphere. GMD008 was  
239 well insulated but still partially followed the outside temperatures with a delay. In the right panel  
240 the total amount of air in the tube is plotted relative to how much it would be if it had the same  
241 pressure and temperature everywhere in the tube as the outside air. Vertical line: the ratio equals  
242 1 if they were the same. During ascent in the troposphere (up to about 10 km) the air in the tube  
243 is warmer, and thus less dense, than outside air. In the tropopause the tube continues to cool so  
244 that the “deficit” becomes smaller, but at higher altitudes, around ~25 km the amount by which  
245 the pressure in the tube is higher than outside becomes substantial relative to the low outside  
246 pressure – as a result the ratio at ~34 km altitude becomes a bit larger than 1. Then, during  
247 descent the outside pressure increases rapidly and the inflow cannot keep up because the  
248 viscosity of air at low pressure is the same as at 1 bar (see section 3). Back in the troposphere the  
249 tube warms up, but much more slowly than outside air. When the tube hits the ground, it is  
250 colder than ambient air temperature so that the ratio is greater than 1.

251 In Figure 3 the fill rate is plotted (mol per hPa of ambient pressure gain) divided by the final fill  
252 (moles of air) at valve closure. At sea level the final pressure is close to 1013 hPa, so that the



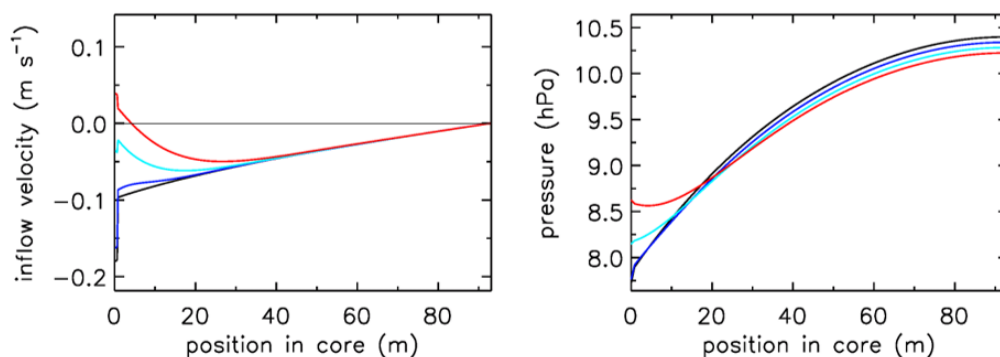
253





254 *Figure 3. Flight of GMD008. The vertical line at  $1.0 \cdot 10^{-3}$  is approximately the expected rate of*  
255 *sample inflow.*

256 the average fraction of final fill per hPa will be approximately 0.001. The uptick upon landing is  
257 the result of a bit of air still entering the tube initially while ambient pressure stops changing,  
258 neglecting high frequency noise. If the valve is not closed quickly this will reverse because as the  
259 tube warms up on the ground, the last air that came in will be expelled. At high altitudes it takes  
260 time for the fill to start because ambient pressure needs to build up enough to force the air in.  
261 The highest altitude was 32.4 km, at 7.7 hPa ambient pressure. The fill starts at 31.6 km and  
262 pressure 8.5 hPa, slowly at first, and gradually becomes faster. To compare the start of fill  
263 between AirCore designs with different diameters and valves, we could take the point at which  
264 the fill rate is  $0.5 \cdot 10^{-3}$ . In this case the “half-fillrate point” is at 27.3 km and ambient pressure of  
265 17.3 hPa. We will see that the fill starts much faster with larger diameters. Figure 4 shows detail



266

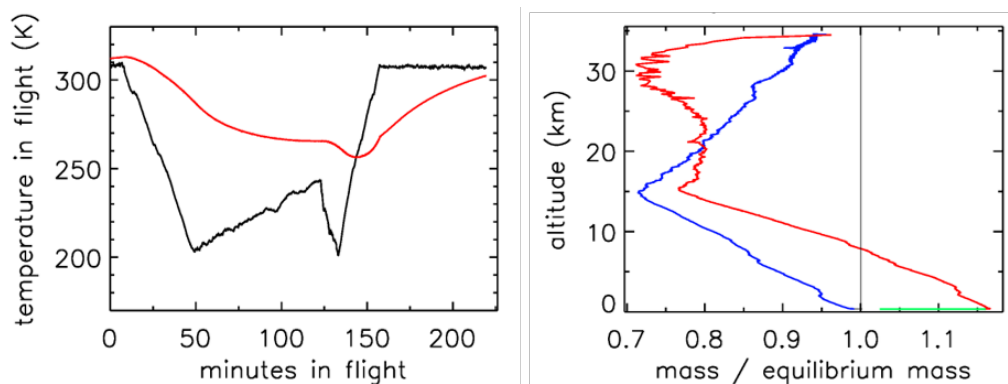
267 *Figure 4. The turnaround at high altitude. Inflow velocity and pressure inside the AirCore from*  
268 *the moment the ascent stops and descent begins. Black, 0 seconds after start of descent; dark*  
269 *blue, 7 s after start; light blue, 14 s; red, 21 s.*

270 of flow and pressure inside the tube for the flight on 20 June 2019 at the start of descent. Initially  
271 the inflow velocity is negative. It is outflow, zero at the closed end and increasing toward the  
272 open end. The velocity has to jump up inside the flow restrictions of the valves and possibly the  
273 dryer at the entrance of the AirCore, adjacent to position at 0 m. After 14 seconds into the  
274 descent (light blue curve) the outflow has weakened considerably and the pressure gradient near  
275 the open end is much smaller. Inflow starts after 19 s, very slowly at first, while at the same time  
276 the flow in most of the tube is still negative (outflow toward the open end), consistent with the  
277 pressure gradients.

278 Let us look now at an AirCore with larger diameters (Figure 5). This one had 26 m of 1/4 inch  
279 (internal diameter 5.84 mm internal diameter) tubing at the open end and 37.6 m of 1/8 inch  
280 (2.67 mm internal diameter) tubing at the closed end, with a total internal volume of 980 cc. In  
281 front of the open end was a valve, the dryer (large magnesium perchlorate particles), and then



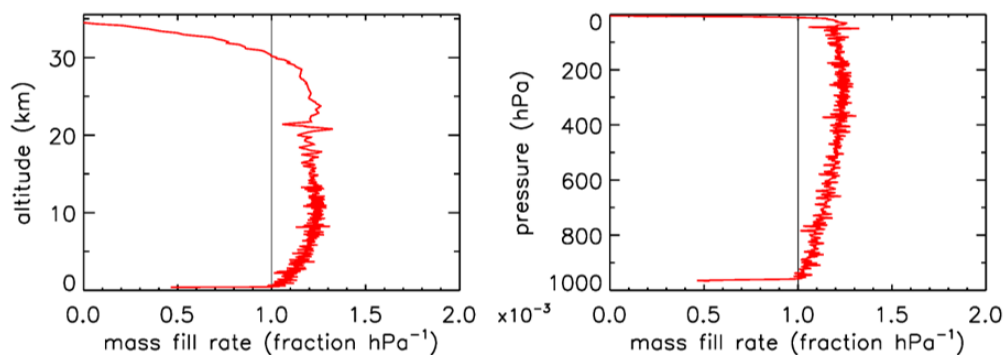
282 another valve connecting to the AirCore tube. It was flown in Oklahoma, U.S. (37.2 N, 97.8 W),  
283 on 23 July 2013. While the AirCore used near Trainou, France, experienced a temperature range



284

285 *Figure 5. Flight of AC01 in Oklahoma. Color scheme in right panel: Blue, ascent; red, descent;*  
286 *green, lying on the ground.*

287 of 15 K, the less well insulated AC01 in Oklahoma saw a range of 57 K. At the moment of  
288 landing the average temperature of the tube was ~40 K cooler than ambient. Fig. 5 shows the  
289 flight data until the moment of valve closure. The valve remained open for 62 minutes after  
290 landing, so that the lowest portion of the atmospheric sample, between pressure altitudes of 844  
291 and 967 mb (1565 to 352 m), was expelled as the AirCore warmed up. The descent started at  
292 34.6 km altitude (4.6 mb). The lowest relative mass deficit (~27%) was reached around 30 km,  
293 in contrast to the Trainou flight with 50% at 27 km altitude respectively. The half-fillrate point of



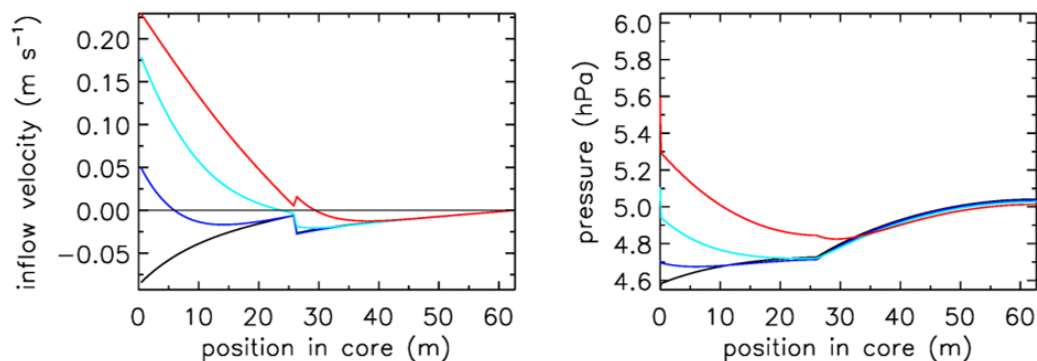
294

295 *Figure 6. Flight of AC01 in Oklahoma. Compare with Figure 3.*

296 0.5 10<sup>-3</sup> per hPa is reached at 33.2 km altitude and 6.2 mb of ambient pressure, a sampling  
297 altitude gain of almost 6 km compared to the Trainou flight. If the total amount of fill air that  
298 remained in the tube is carefully measured that would give an independent determination of the  
299 half-fillrate point estimated here. The fill rate below ~8 km falls off noticeably as the warming



300 rate of the tube speeds up. The negative mass fill rate while on the ground cannot be portrayed in  
301 Fig. 6 because ambient pressure remains constant. This AirCore design contains a larger fraction  
302 of stratospheric air than GML008, mostly because of the wider diameter, but also because it was  
303 allowed to cool more.



304

305 *Figure 7. Flight of AC01 in Oklahoma, showing inflow velocity Compare with Figure 4. Black, 0*  
306 *seconds after start of descent; dark blue, 2 s after start; light blue, 5 s; red, 10 s. Note the much*  
307 *smaller delay than in Fig.4. The flow velocity inside the valves and dryer has not been plotted*  
308 *here, but the pressure drop across them has.*

309 If one wants to sample still higher into the stratosphere the diameter of the first 10 to 20 m at the  
310 open end needs to be widened further. All of this is consistent with Fig. 7, where we also see that  
311 at the start of the descent the outflow velocity inside the tube drops by a factor of ~4 when,  
312 moving from the back to the open end, at 26 m the tube diameter becomes wider by a factor of 2.  
313 This applies of course also to the inflow as shown by the red curve. At the same point the  
314 pressure gradient becomes less steep by the same factor of 4. The fill starts at ambient pressure  
315 of 4.7 mb. We also note that in this case the pressure drop inside the two valves and the dryer is a  
316 large part of the overall pressure drop across the entire tube, especially when the tube diameter is  
317 larger.

318 In these calculations we have experimented with another strategy to fill the AirCore. One could  
319 launch it with both valves open, but the one in the back is closed as soon as the descent starts.  
320 That would decrease the amount of fill air that remains in the back. However, the difference from  
321 having the back valve closed during the entire flight is minuscule.

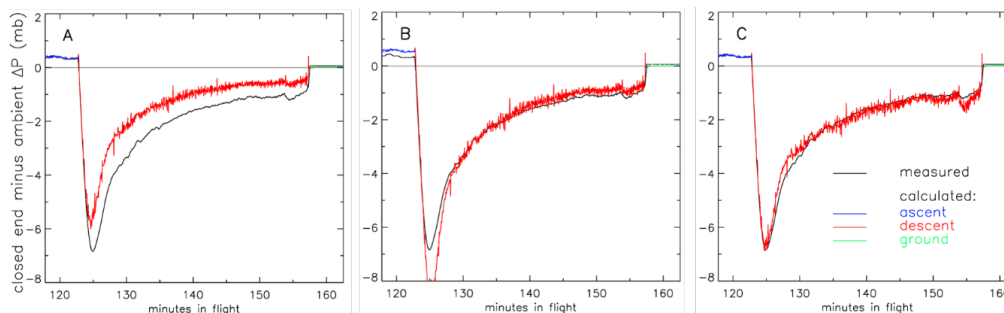
322

## 323 5. Valves

324 So far the treatment of valves and the dryer has been missing from this description. As a first  
325 approximation we could treat the valves as short pieces of tubing with reasonably “average”  
326 internal diameter and length such that their internal volume is correct. This does not provide



327 enough flow resistance, when we compare it to differential pressure measurements made during  
 328 some flights between the closed end of the AirCore and the outside ambient air (Figure 8).



329

330 *Figure 8. Pressure difference ( $\Delta P$ ) between closed end of tube and outside air during the*  
 331 *descent portion of flight of AC01 in Oklahoma as a function of elapsed time in flight. Black:*  
 332 *measured pressure difference (mb, or hPa). Red: calculated  $\Delta P$  with three different treatments of*  
 333 *the valves. A, fixed internal diameter and length; B, same as in A, but optimized; C, using*  
 334 *optimized  $C_v$  and  $X_{TPR}$  (see text) values.*

335 In panel A we calculate that during the descent the air enters the tube too easily, so that the  
 336 altitudes assigned to the air sample in the stratosphere would be biased high. We could decrease  
 337 the chosen internal average diameter of the valves (panel B), optimized so that the difference  
 338 between calculated and measured  $\Delta P$  during the entire descent, from minute 123 to 157, is  
 339 minimized. However, it is clear that this effective or apparent internal diameter needs to change  
 340 during the flight. Using  $C_v$  values and a description of choked flow is clearly better. In panel C  
 341 we have chosen the  $C_v$  and  $X_{TPR}$  values such that the average difference from minute 123 to 157  
 342 is zero and the standard deviation of differences is minimized. This implicitly includes any  
 343 effects caused by the dryer in between the two valves.

344 The flow inside a valve can be complicated, with sharp corners, turbulence, sudden acceleration  
 345 through a flow restriction with its associated heating and cooling of the gas, etc. The industry has  
 346 introduced flow coefficients ( $C_v$  in the U.S., and  $K_v$  elsewhere) as an empirical approach to flow  
 347 calculations, as in the Swagelok brochure (2020). The expressions for air, slightly generalized  
 348 from Swagelok, for gas flow are as follows. For low pressure drop flow, we have

349 
$$Q_n = 6950 C_v P_1 \left(1 - \frac{X}{3 X_{TPR}}\right) \sqrt{\frac{X}{T_1}} \quad (\text{Eq. 5a}),$$
 where  $Q_n$  is in liters per minute at standard

350 conditions of 1 bar and 0°C,  $P_1$  and  $T_1$  are pressure (bar) and temperature (Kelvin) upstream of  
 351 the valve,  $\Delta P$  is the pressure drop across the valve,  $X$  is the pressure drop ratio  $\Delta P/P_1$ , and  $X_{TPR}$   
 352 is the terminal pressure drop ratio between (0 and 1) above which we have choked flow. Under  
 353 choked flow conditions the flow is fully independent of  $P$  and  $T$  downstream of the valve. It is  
 354 also important to know that the flow coefficient  $C_v$  is not a pure number, but has physical  
 355 quantities and units embedded in it.



356 For a high pressure drop ( $X > X_{\text{TPR}}$ ), we have

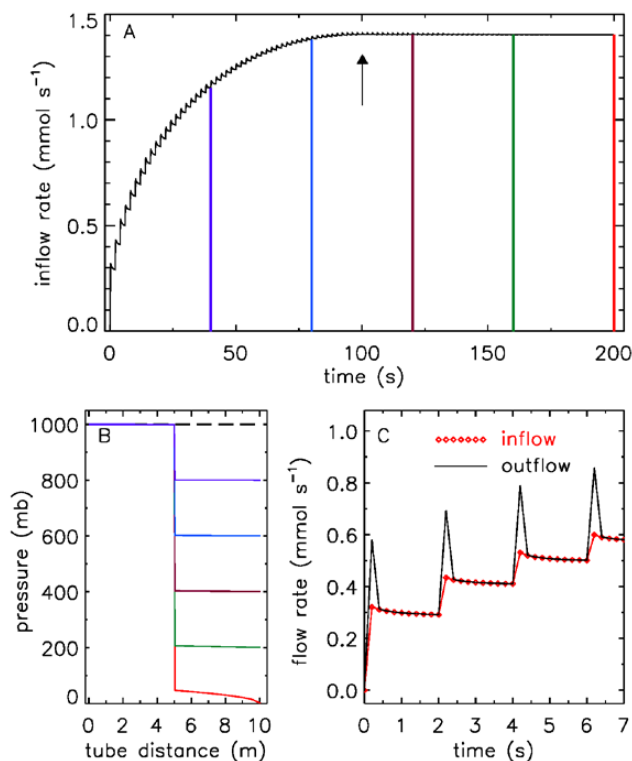
357 
$$Q_n = 6950 C_v P_1 \frac{2}{3} \sqrt{\frac{X_{\text{TPR}}}{T_1}} \quad (\text{Eq. 5b}),$$
 which is obtained from the previous expression by

358 substituting  $X_{\text{TPR}}$  (a constant) for  $X$ . In these expressions we prefer to express the flow, instead  
359 of in standard L/min as in the Swagelok brochure, as 0.04403 mol/min. This is the same, when  
360 using the molecular weight of dry air (28.97 g/mol), as a mass flow of 1.276 g/min.

361 In Fig. 8C we optimized both  $C_v$  and  $X_{\text{TPR}}$  to get the best match for the calculated pressure  
362 difference across the AirCore with the observed history during the descent. The value of  $X_{\text{TPR}}$   
363 depends on valve design, and may not be the same when flow goes in the opposite direction.  
364 Many valves have an arrow for flow direction printed on them. For most AirCore flights  
365 differential pressure measurements have not been recorded. But the valves (and also driers) could  
366 be tested with a standard procedure (see Figure 9 as one example). Alternatively, or as a  
367 complementary check, a micro-spiking method during filling could be used (Wagenhäuser,  
368 2021).

369 Figure 9 shows a potential test procedure for determining  $C_v$  and  $X_{\text{TPR}}$  values. The figure is  
370 drawn using the two expressions for  $Q_n$  above, for low flow and choked flow. Starting from a  
371 uniform pressure of 1 bar, the pressure at the downstream side is lowered in 10 mb steps, at 2 s  
372 intervals. In this example  $C_v = 0.01$  and  $X_{\text{TPR}} = 0.5$ , so that the transition to choked flow occurs  
373 at a pressure drop of 0.5 bar (panel A, upward arrow at 100 s). When the pressure at 10 m  
374 approaches zero, the flow speed is high, causing a significant pressure drop between 5 and 10 m.

375



376

377 *Figure 9. A potential test procedure to determine  $C_v$  and  $X_{TPR}$  values for valves. In this example*  
378 *there is 5 m of 1/4" tubing on each side. Outflow at the 10 m point (black curve) is shown in*  
379 *panels A and C. There is a flow pulse at every step because the downstream 5 m section empties*  
380 *quickly. The time resolution is 0.2 s. Inflow at 0 m is shown as red diamond symbols in panel C.*  
381 *Panel B, pressure in the tube from time 0 (dashed line) at 40 s intervals, corresponding to the*  
382 *colors in panel A.*

383

## 384 6. Mixing inside the tube

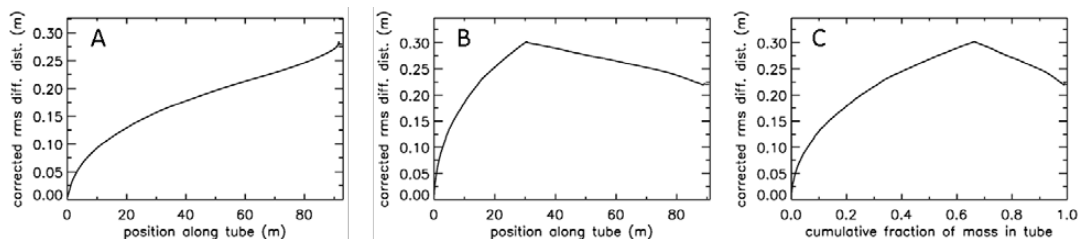
385 The fill dynamics calculation has produced time series of air density, pressure and temperature,  
386 and flow velocity everywhere in the tube as a function of time, from the start of the fill process,  
387 which begins a varying amount of time after the AirCore has started its descent, to the time of  
388 valve closure. We divide the final amount of air in the tube at closure into 400-500 equal mass  
389 packets. Starting from 400 we increase the number, which shrinks the size of each packet, until  
390 the remaining fill air in the back of the tube comprises an exact integer number of packets. For  
391 each mass packet, after it has entered the tube we follow it through the tube, as it is pushed  
392 toward the back while being compressed by packets entering later. The time steps are defined by  
393 when a new packet has fully entered, and they are longer at the start of the fill. The molecular



394 diffusivity  $D$  and the Taylor diffusivity  $D_T$  are different at each step. However, the amount of  
 395 spreading of a packet calculated at each time step “ $k$ ” is decreased as the increasing pressure  
 396 compresses the packet further. So the contribution of each step to the final spreading at valve  
 397 closure is calculated by dividing the density during that time step by the final density in the tube.  
 398 We are thus accumulating the “ $2Dt$ ” term of  $X_{rms} = (2Dt)^{0.5}$ , with Taylor diffusion added:

$$399 \quad X_{rms} = \sqrt{2 \sum_k (D_k + D_{T,k}) \frac{\rho_k}{\rho_{final}} t_k} \quad \text{Eq. 6}$$

400 For an AirCore with (almost) uniform diameter we get mixing as in Fig. 10 A. Close to the open  
 401 end at position 0 m, there is very little mixing because the time to mix was short. Near the closed  
 402 end at 93 m the spread of mixing deviates from what see in the first approximately 2/3 of the  
 403 tube because the fill started slowly, giving extra mixing time for the high altitude samples that  
 404 were later pushed to the back.



405  
 406 *Figure 10. Root-mean-square diffusive mixing when the valve at position 0 is closed. Panel A,*  
 407 *Flight of GMD008 in Trainou. Panel B, the same flight data, but used to calculate the filling of a*  
 408 *different AirCore, with 30.9 m of 1/4” tubing at the open end, and 60.1 m of 1/8” at the closed*  
 409 *end. Panel C, same as B, but plotted as cumulative fraction of total mass, from 0 to 1.*

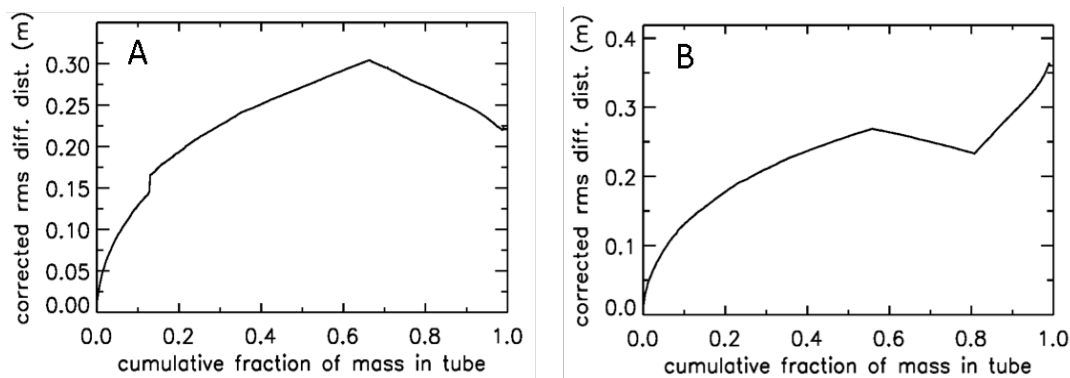
410 For an AirCore with two sections of different diameter we see an interesting effect (Fig.10 B).  
 411 The air that comes in at high altitudes and ends up in the back of the tube, has to go through  
 412 the 1/4” section first. When a packet enters the 1/8” section, its spread becomes approximately  
 413 four times larger, while its  $2Dt$  accumulation term stays the same. Approximately, because the  
 414 inner diameters (ID) matters, not the outer (OD). To correct for the jump we add another factor  
 415 to Eq. 6, and we will call this corrected rms diffusion distance:

$$416 \quad X_{rms} = \sqrt{2 \sum_k (D_k + D_{T,k}) \frac{\rho_k}{\rho_{final}} \frac{(dvol/dx)_k}{(dvol/dx)_{ref}} t_k} \quad \text{Eq. 7}$$

417 In Eq. 7  $dvol/dx$  is the increment in volume per increment in length of the tube, while  $(dvol/dx)_{ref}$   
 418 is the total volume divided by the total length, both in units of  $m^2$ . This prevents a jump at the 30  
 419 m position, but more importantly, what matters for mixing is the spread relative to total mass in  
 420 the tube, not whether it is in the 1/4 or 1/8” section. From now on we call this configuration “1/4  
 421 -1/8”. Fig. 10 B shows that air closer to the back has been in the 1/4” section for a shorter time,



422 and thus experienced less mixing relative to mass. When plotting mixing not as a function of  
423 position, but as a function of cumulative mass in the tube, Fig 10 C also shows that the 1/8”  
424 section contains approximately 1/3 of the total air sample.



425  
426 *Figure 11. Two additional cases of mixing upon valve closure. Panel A, same AirCore 1/4 -1/8,*  
427 *but the flight data have been changed. Panel B, same flight data as in Fig. 10A, but the AirCore*  
428 *configuration is 1/4 - 1/8 - 1/4.*

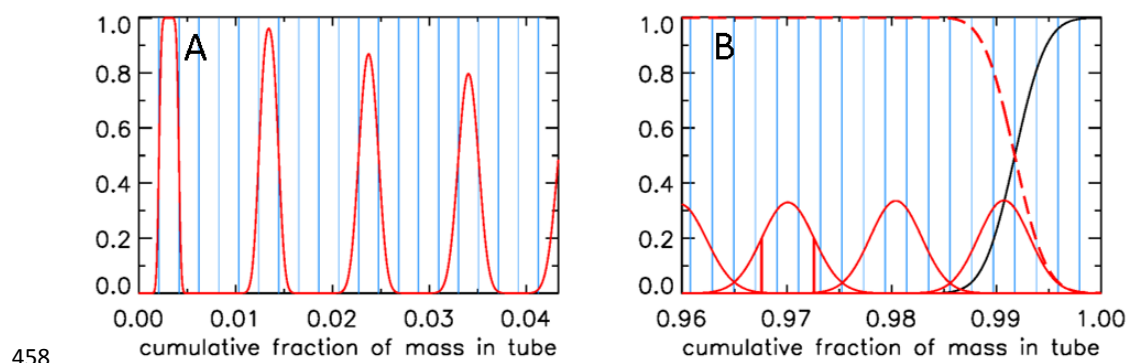
429 In Fig. 11A when the tube had descended to 850 mb, the atmospheric pressure data were  
430 changed to simulate an updraft (lowering outside pressure) followed by a downdraft. The most  
431 recent 7 mass packets were lost from the tube during the updraft, and replaced by new air during  
432 the downdraft (above average rate of increase of outside pressure). As a result, the air sample  
433 that just escaped from being lost is now adjacent to the replacement air, creating the jump in rms  
434 mixing because it has been ~15 s longer in the tube than the first replacement air entering. In Fig.  
435 11B the AirCore has now three sections, from the open to the closed end, first 30.1 m of 1/4”,  
436 then 52.1 m of 1/8”, and 10.1 m of 1/4” diameter, which we will call “1/4 - 1/8 - 1/4”. This was  
437 done solely to illustrate clearly the effects of using different diameters. Similar to what we saw in  
438 Fig. 10A, the spread of mixing steepens near the closed end. Also those samples resided not long  
439 enough in the 1/8” section to have much benefit in terms of slowing down the mixing, but  
440 between 0.80 and 0.85 they had been long enough in the 1/8” section to have experienced less  
441 mixing than air ending up at the 0.57 point, the first transition between 1/4 and 1/8”.

442 We will now express the amount of spreading (in both directions – twice the rms distance) of  
443 each equal-mass “packet” of air as a fraction of the total mass of air in the tube, assuming that  
444 the temperature inside the tube has become uniform. If that fraction were 0.01 everywhere in the  
445 tube there would be slightly less than 100 independent samples in the AirCore. Slightly less  
446 because the remaining fill air in the back takes up space. Figure 12 shows a more realistic  
447 situation. Each sample takes up the same volume, separated by the blue vertical lines, producing  
448 vertical boxes. If there is almost no mixing, as in the case of the last sample that entered the  
449 AirCore, the sample almost completely fills the first volume (or box in Fig. 12A), which is  
450 indicated by the value 1.0 on the y-axis. The red curve centered on the second box has started to



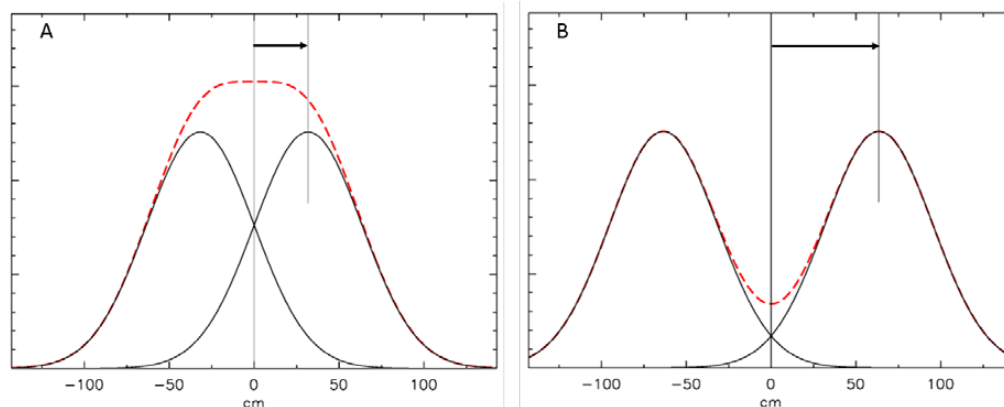


451 “leak” some sample into the adjoining boxes. The next samples shown are the 7<sup>th</sup>, 12<sup>th</sup>, and 17<sup>th</sup>.  
452 For the latter, the sample is just starting to leak into boxes 15 and 19. To plot the start of this  
453 process correctly, each packet is subdivided into 13 equal portions. Narrow Gaussian spreading,  
454 slowly increasing further into the tube, is calculated for each portion, and then summed. The  
455 width of each Gaussian is shown in figure 10C as a function of fraction of cumulative mass in  
456 the tube, and the area of each curve is 1/13 of the area of the box. This produces a constant value  
457 of 1.0 in the center and only the outer portions reach into the neighboring boxes.



458  
459 *Figure 12. A, Mixing of individual air “packets” (red) near the open end with their neighbors*  
460 *after valve closure for the case shown in Fig. 10C; B, mixing near the closed end (red), vertical*  
461 *red lines centered on 0.97 show the  $\pm 1 \sigma$  points, black curve is remaining fill air, and the sum of*  
462 *all actual sample packets, also of those not shown, is the red dashed line.*

463 In Fig. 12B we plot the situation near the closed end. As in Fig. 12A, the mixing of only every  
464 fifth air packet is plotted, here ending with the first that came in at the highest altitude, centered  
465 approximately at 0.991. The remaining fill air in this case has the mass of four packets, and the  
466 curves of fill air and of the total air sample (sum of all packets) cross over at exactly the point  
467 where the fourth box from the right starts. How we calculate mixing at a closed end (at  $x = 0$ ) is  
468 shown in Fig. 13.



469

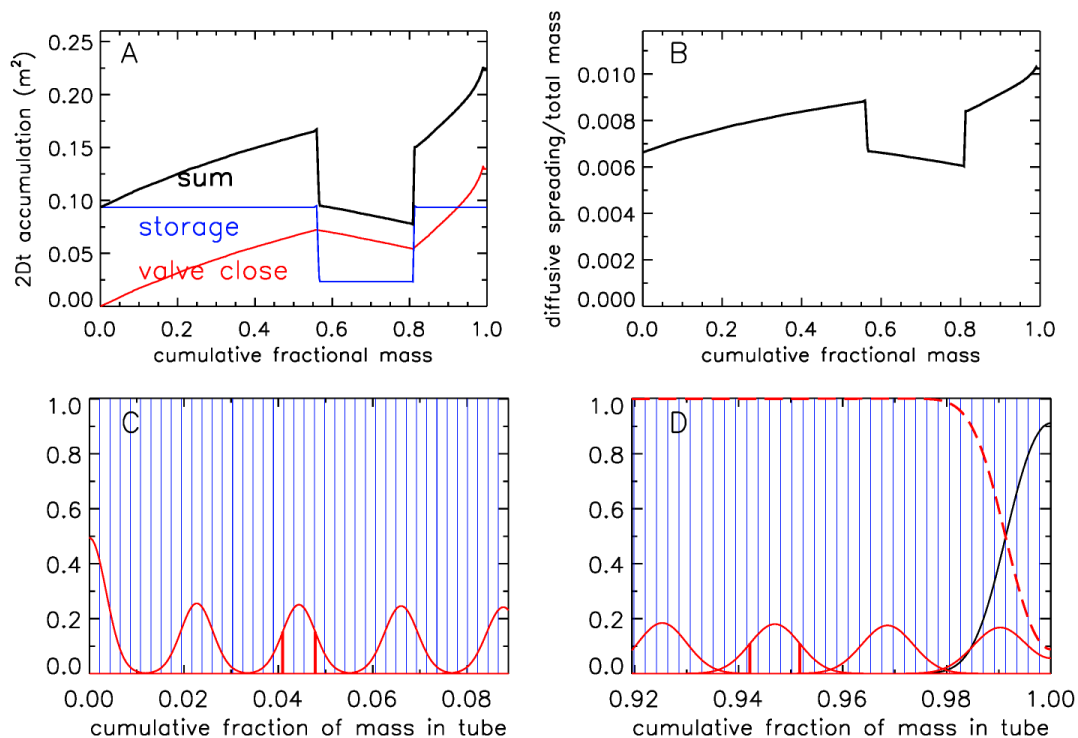
470 *Figure 13. Mixing at a closed end. The Aircore is to the right of the zero centimeter point. A, the*  
471 *distribution of mixing started one hour ago from a plane at 31.8 cm (one root-mean-square of*  
472 *the distribution), indicated by the arrow. A fictitious “mirror” distribution is centered at -31.8*  
473 *cm. The red dashed curve is the sum of the two distributions; B, same calculation, but the center*  
474 *of the distribution is twice as far from the end as in A.*

475 Diffusive mixing that would be to the left of  $x = 0$ , is reflected toward positive values of  $x$ . The  
476 slope of the distribution must be zero at  $x = 0$  because any non-zero slope would imply a  
477 diffusive flux out of, or into, the tube. This is conveniently modeled by assuming a fictitious  
478 distribution mirrored relative to  $x = 0$ , then the two are added, and the portion of the sum for  
479 positive values of  $x$  represents the mixing distribution near a closed end.

480 Let us assume that after the valve has been closed there has been a half hour delay before  
481 analysis starts. Therefore, additional diffusion has taken place, as shown in Fig. 14 for the case  
482  $1/4 - 1/8 - 1/4$  (Figure 11B). The  $2Dt$  term has been increased by an amount dependent on the  
483 diameter of the tube, normalized as in Eq. 7. In the upper right (panel B) the square root of the  
484 sum has been taken, and then transformed into the spreading width relative to total mass in the



485

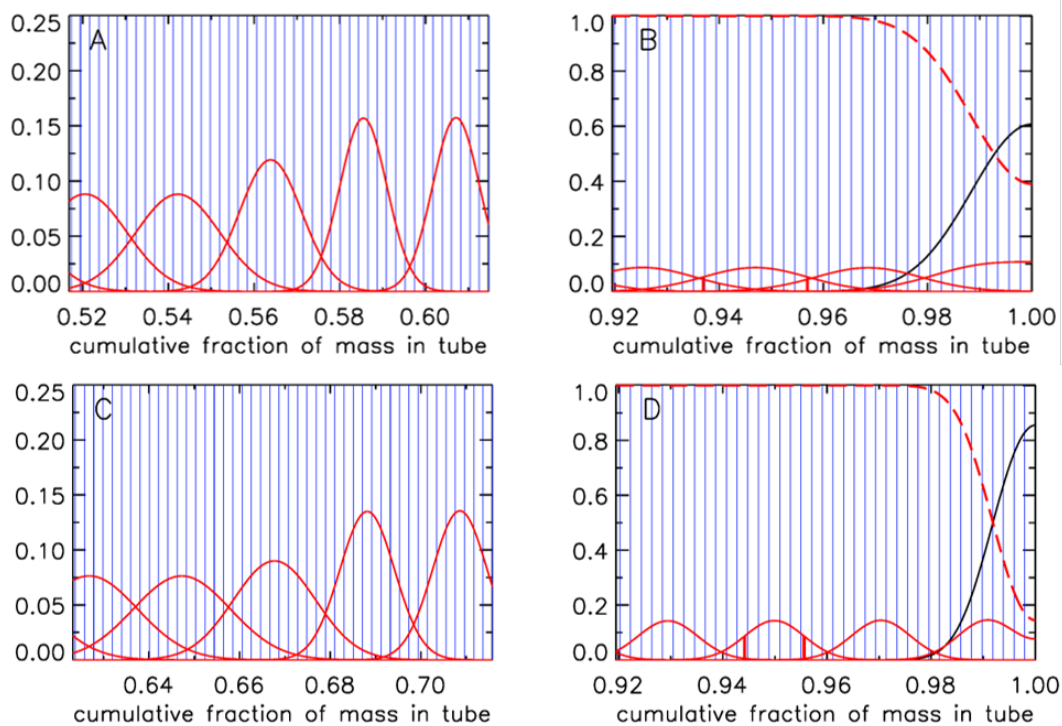


486

487 *Figure 14. Mixing after 30 minutes of storage, for AirCore 1/4 - 1/8 - 1/4. A, Sum (black) of the*  
488 *2Dt accumulation during the flight (red) and during storage (blue), in units of  $m^2$ ; B, spreading*  
489 *width expressed as a fraction of total mass in the tube; C, amount of spreading near what was*  
490 *the open end, for clarity only every 10<sup>th</sup> packet is shown; D, same, near the closed end. Vertical*  
491 *red lines show the  $\pm 1 \sigma$  distances from the peak.*

492 tube. The width is defined here as the distance between the  $\pm 1 \sigma$  points of the Gaussian which  
493 contains  $\sim 68\%$  of the probability distribution, shown in Fig. 14C at  $x = 0.0410$  and  $0.0478$   
494 around the center at  $x = 0.0444$ , and in fig. 14D at  $x = 0.9422$  and  $0.9518$  around the center at  $x =$   
495  $0.9470$ . These numbers correspond to the full widths shown in fig. 14B. The last packet to enter  
496 the tube is centered at  $x = 0.0011$  and  $1 \sigma = 0.0033$ . Most of the diffusive spreading is to the  
497 right, so that the peak is almost twice as high and the full width a little over half as wide as the  
498 one centered on  $x = 0.023$ .

499 Often the AirCore is analyzed significantly later than 30 min. after valve closure, and the  
500 measurement process itself may take half an hour. In Figure 15 the state of mixing four hours  
501 after valve closure has been calculated, and two AirCore configurations are compared. The



502

503 *Figure 15. Mixing after 4 hours of storage. A, at the transition from 1/4" diameter to 1/8", for*  
504 *AirCore 1/4 - 1/8 - 1/4; B, near closed end, for 1/4 - 1/8 - 1/4; C, at the transition from 1/4"*  
505 *diam. to 1/8", for AirCore 1/4 - 1/8; D, near closed end, for 1/4 - 1/8.*

506 spreading width of air “packets” near the closed end is nearly twice as large for the 1/4 - 1/8 –  
507 1/4 case as for the 1/4 - 1/8 case, and the initial fill air penetrates almost 50% further into the  
508 tube. It would in most cases not be a good idea to have a wide bore section at the closed end. If  
509 one waits 24 hours (6 times longer) before starting the analysis, the spreading width near the  
510 closed end, centered at  $x = 0.9470$ , is 2.32 times larger than after 4 hours, not quite  $\sqrt{6}$  because  
511 after 4 hours the spreading that occurred during the descent still makes a small, but still  
512 noticeable, contribution.

513

## 514 7. Potential information content of the AirCore

515 When the air is slowly pushed through an analyzer, we obtain a continuous curve for the mole  
516 fraction of the gases of interest as a function of fractional cumulative mass in the tube which is  
517 linked to flight data such as pressure altitude, geometric altitude, latitude, longitude, etc. as  
518 calculated from the filling dynamics. We define the information content as the number of  
519 independent air samples that are inside the tube, or the number of degrees of freedom (DoF).



520 Longer wait times before analysis decrease DoF, but it could be decreased further by additional  
 521 mixing in the measurement cell, or by successive analyzer cells measuring different gas species.  
 522 In the section above we chose more than 400 equal mass packets to calculate mixing. This was  
 523 done to prevent a possibly low numerical resolution of the mixing calculation which would  
 524 unnecessarily create a low bias in DoF estimates. Ideally, the measurement process could be  
 525 modeled in a way similar to the fill and mixing calculation above, convolving the packets  
 526 leaving the AirCore with a pulse response of the measurement cell. The response could be  
 527 measured separately by introducing a sharp spike just before the cell, and recording how it is  
 528 mixed and flushed out. This would be similar to the spiking method described by Wagenhäuser  
 529 et al. (2021). In the worst case the measurement cell would be perfectly mixed giving rise to  
 530 exponential flushing. After one cell volume has entered from the AirCore into the measurement  
 531 cell, the latter still contains a fraction  $1/e$  of what went through the cell before, so that the new  
 532 volume comprises  $(1 - 1/e) = 0.63$  of the cell loading. On the other hand, “plug flow” (like in the  
 533 AirCore itself) would produce very little additional mixing, but there could still be some  
 534 turbulent eddies near the entrance and exit of the cell. The actual influence of the measurement  
 535 cell on mixing lies somewhere in between those two extremes.

536

## 537 8. Numerical implementation

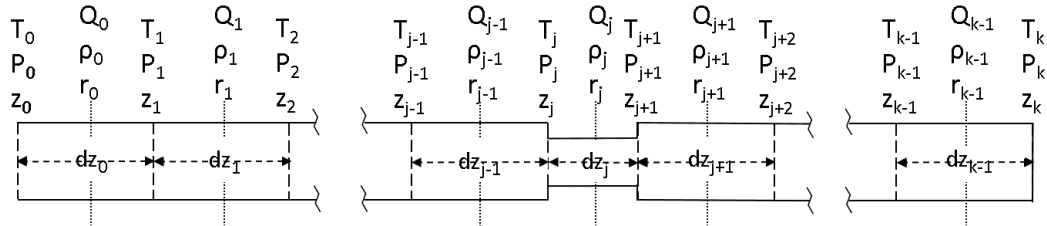
538 The AirCore can consist of one or more sections of different length, each with a different inner  
 539 diameter. For example, GML has flown AirCores with a wider bore at the open end and a narrow  
 540 bore at the closed end, in order to get better vertical resolution for the stratosphere. The sections  
 541 can be divided into a number of smaller segments when Eq. 2 is discretized for numerical  
 542 solution (Figure 16):

$$543 \quad Q = -\rho \frac{\pi r^4}{8\eta} \frac{dP}{dz} \Rightarrow Q_j = -\frac{P_j + P_{j+1}}{R(T_j + T_{j+1})} \frac{\pi r_j^4}{8\eta_j} \frac{P_{j+1} - P_j}{dz_j}$$

544  $Q_j$  is centered in the middle of segment  $dz_j$ . The first factor in  $Q_j$  is the average amount density  
 545 ( $\rho_j$ ). The pressure change at the boundary between segments  $dz_{j-1}$  and  $dz_j$  caused by the  
 546 imbalance of the flows  $Q_{j-1}$  and  $Q_j$  is equal to that imbalance divided by the volume between the  
 547 mid points of  $dz_{j-1}$  and  $dz_j$ . Adding in the pressure change due to temperature (Eq. 2) we get for  
 548 the change at boundary  $j$ :

$$549 \quad \frac{dP_j}{dt} = \frac{P_j}{T_j} \frac{dT_j}{dt} + \frac{T_j}{0.5(dz_{j-1}r_{j-1}^2 + dz_jr_j^2)} \frac{P_j + P_{j+1}}{T_j + T_{j+1}} \frac{r_j^4}{8\eta_j} \frac{P_{j+1} - P_j}{dz_j}$$

$$550 \quad - \frac{T_j}{0.5(dz_{j-1}r_{j-1}^2 + dz_jr_j^2)} \frac{P_{j-1} + P_j}{T_{j-1} + T_j} \frac{r_{j-1}^4}{8\eta_{j-1}} \frac{P_j - P_{j-1}}{dz_{j-1}} \quad \text{Eq. 8}$$



551

552 *Figure 16. Coordinate system in the AirCore. The coordinate along the length of the tube is  $z$  (m).*  
 553 *There are  $k$  segments, starting from the open end at  $z_0$  to the closed end at  $z_k$ , between the*  
 554 *vertical dashed lines. Amount flow ( $Q_n$ , mol  $s^{-1}$ ), amount density  $\rho_n$  (mol  $m^{-3}$ ), simply written as*  
 555  *$Q$  and  $\rho$  from here on out, are defined in the middle of each segment, pressures ( $P$ ) and*  
 556 *temperatures ( $T$ ) are defined at the borders of each segment. The length ( $dz$ ) as well as radius*  
 557 *( $r$ ) of the segments may differ.*

558 The first term  $(P/T)(dT/dt)$  is handled separately from the two other terms describing the amount  
 559 change. We write the latter two with the time step going from  $n$  to  $n+1$  (superscript):

$$560 \quad P_j^{n+1} - P_j^n = \left[ \frac{2T_j^n (P_{j+1}^n + P_j^n)}{T_{j+1}^n + T_j^n} \frac{r_j^4}{\eta_j} \frac{P_{j+1}^{n+1} - P_j^{n+1}}{dz_j} \right. \\ 561 \quad \left. - \frac{2T_j^n (P_{j-1}^n + P_j^n)}{T_{j-1}^n + T_j^n} \frac{r_{j-1}^4}{\eta_{j-1}} \frac{P_j^{n+1} - P_{j-1}^{n+1}}{dz_{j-1}} \right] \frac{t^{n+1} - t^n}{8(dz_{j-1}r_{j-1}^2 + dz_jr_j^2)} \quad \text{Eq. 9}$$

562 On the right hand side we have defined the pressure *differences* at the *end* of the time step. The  
 563 reason is to make the solution of the matrix equation described below unconditionally stable.  
 564 This method has been described as “fully implicit” or “backward time” (Press, 1992). We leave  
 565 the pressure and temperature *averages* as defined at the start of the time step. They determine the  
 566 average amount density of the air and do not create any numerical instability. Eq. 9 can be  
 567 further re-arranged, for  $j=1$  to  $k-1$ , as

$$568 \quad P_j^n = - \frac{t^{n+1} - t^n}{8(dz_{j-1}r_{j-1}^2 + dz_jr_j^2)} \left[ \frac{2T_j^n (P_{j+1}^n + P_j^n)}{T_{j+1}^n + T_j^n} \frac{r_j^4}{\eta_j dz_j} \right] P_{j+1}^{n+1} + \\ 569 \quad \left( 1 + \frac{t^{n+1} - t^n}{8(dz_{j-1}r_{j-1}^2 + dz_jr_j^2)} \right) \left[ \frac{2T_j^n (P_{j+1}^n + P_j^n)}{T_{j+1}^n + T_j^n} \frac{r_j^4}{\eta_j dz_j} + \frac{2T_j^n (P_{j-1}^n + P_j^n)}{T_{j-1}^n + T_j^n} \frac{r_{j-1}^4}{\eta_{j-1} dz_{j-1}} \right] P_j^{n+1} \\ 570 \quad - \frac{t^{n+1} - t^n}{8(dz_{j-1}r_{j-1}^2 + dz_jr_j^2)} \left[ \frac{2T_j^n (P_{j-1}^n + P_j^n)}{T_{j-1}^n + T_j^n} \frac{r_{j-1}^4}{\eta_{j-1} dz_{j-1}} \right] P_{j-1}^{n+1} \quad \text{Eq. 10}$$

571 This is a tridiagonal matrix equation,  $\mathbf{A} \bullet \mathbf{P}^{n+1} = \mathbf{P}^n$ , linking the  $k+1$  dimensional pressure vector  
 572  $\mathbf{P}^{n+1}$  at the end of the time step to the pressure vector  $\mathbf{P}^n$  at the start of the time step. The solution



573 is  $P^{n+1} = \mathbf{A}^{-1} \cdot P^n$ , in which  $\mathbf{A}^{-1}$  is the inverse matrix calculated by the subroutine TRISOL which is  
 574 the IDL version of TRIDAG described by Press et al (1992). If the tube is closed at  $z = 0$ , then in  
 575 the first line of  $\mathbf{A}$  the first (diagonal) and second (above the diagonal) element (all others are  
 576 zero) are respectively

$$577 \quad 1 + \frac{t^{n+1} - t^n}{8(dz_0 r_0^2)} \frac{2T_1^n (P_1^n + P_0^n)}{T_1^n + T_0^n} \frac{r_0^4}{\eta_0 dz_0} \quad \text{and} \quad - \frac{t^{n+1} - t^n}{8(dz_0 r_0^2)} \frac{2T_1^n (P_1^n + P_0^n)}{T_1^n + T_0^n} \frac{r_0^4}{\eta_0 dz_0}$$

578 If the tube is open at  $z = 0$ , then the first element of the first line equals 1, and all others are zero.  
 579 In this case  $P_0$  is defined at all times by the outside atmospheric pressure, or by a defined  
 580 pressure from a cylinder. There is no influence from any place inside the tube. The algorithm  
 581 also allows the other end to be either closed or open to outside air. If closed, then the last two  
 582 elements of the  $(k+1)^{\text{st}}$  row are respectively

$$583 \quad - \frac{t^{n+1} - t^n}{8(dz_{k-1} r_{k-1}^2)} \frac{2T_{k-1}^n (P_{k-1}^n + P_k^n)}{T_{k-1}^n + T_k^n} \frac{r_{k-1}^4}{\eta_{k-1} dz_{k-1}} \quad \text{and}$$

$$584 \quad 1 + \frac{t^{n+1} - t^n}{8(dz_{k-1} r_{k-1}^2)} \frac{2T_{k-1}^n (P_{k-1}^n + P_k^n)}{T_{k-1}^n + T_k^n} \frac{r_{k-1}^4}{\eta_{k-1} dz_{k-1}}$$

585 If both sides are open, each with a different defined constant pressure, then after an initial  
 586 transient the flow settles to steady state flow corresponding to Poiseuille's equation.

587 This describes the core algorithm, of which there are two versions, called tubeflowstep3.pro and  
 588 tubeflowstep3Cv.pro. They have been programmed in Interactive Data Language (IDL). These  
 589 algorithms have the flexibility to accommodate segments of the tube that have different lengths  
 590 as well as diameters, flows in both directions, one or two valves open, a temperature gradient  
 591 along the tube with its corresponding viscosity gradient, and variable time steps. Another  
 592 routine, called analyzefill\_Gaus\_ict.pro, reads the lengths and diameters of tube sections, valves  
 593 and dryer, and the relevant flight data, namely outside air pressure and temperature, the  
 594 temperature of the AirCore at different locations along the tube, all as a function of time. If  $C_v$   
 595 and  $X_{\text{TPR}}$  values of valves are defined they will be used. In that case tubeflowstep3Cv.pro nudges  
 596 the apparent internal diameter of one or more valves for a given flow toward satisfying Eq. 5 (see  
 597 section 5). This needs to be iterated because when we change the internal valve diameter the  
 598 pressures and flows will then adjust elsewhere in the tube. The analyzefill\_Gaus\_ict program  
 599 also reads altitude, latitude, and longitude, but they are not needed for the flow dynamics  
 600 calculation per se. It sets up the coordinate system and initializes variables. By calling  
 601 tubeflowstep3.pro at every time step, or tubeflowstep3Cv.pro if  $C_v$  and  $X_{\text{TPR}}$  values are defined,  
 602 it calculates the pressure in the tube, the amount of air and the amount flow, and the flow  
 603 velocity, all as a function of time and location in the tube. This is how altitude, pressure altitude,  
 604 latitude, and longitude are tied to position in the tube. The \_Gaus portion of the name indicates



605 that Gaussian mixing is used as described in this paper, and \_ict indicates that the program  
606 expects the needed information about the tube and the flight in the ICARTT format.

607 Although developed simultaneously with analyzefill\_Gaus\_ict.pro for the passively filled  
608 AirCore, the tubeflowstep3Cv program can also be used to model flow when the AirCore is  
609 actively filled with a pump and some form of flow and pressure control. In that case a program  
610 equivalent to analyzefill\_Gaus\_ict.pro would need to be developed.

611 The code in analyzefill\_Gaus\_ict.pro also produces diagnostic graphics showing how the fill  
612 proceeded. In fact, all figures in this paper have been produced by analyzefill\_Gaus\_ict.pro  
613 except for Figure 9.

614

#### 615 **Acknowledgement**

616 I thank Anna Karion, Colm Sweeney, Tim Newberger, Jack Higgs, Sonja Wolter, and Bianca  
617 Baier for making our lab's AirCore program blossom. Especially the controlled return is a very  
618 promising improvement over the return by parachute.

619

620 The programs are available at ....

621

#### 622 **References**

623 Battle, M., M. Bender, T. Sowers, P. Tans, J. Butler, J. Elkins, J. Ellis, T. Conway, N. Zhang, P.  
624 Lang, and A. Clarke (1996), Atmospheric gas concentrations over the past century measured in  
625 air from firn at the South Pole, *Nature* 383, 231-235.

626 Berg, R. (2005), Simple flow meter and viscometer of high accuracy for gases, *Metrologia* 42,  
627 11-23.

628 Chapman, S. and T. Cowling (1970), *The mathematical theory of non-uniform gases*, 3<sup>rd</sup> edition,  
629 Cambridge University Press.

630 Jeans, J. (1952), *An introduction to the kinetic theory of gases*, Cambridge Univ. Press.

631 Kadoya, K., N. Matsunaga, and A. Nagashima (1985), Viscosity and Thermal Conductivity of  
632 Dry Air in the Gaseous Phase, *J. Phys. Chem. Ref. Data* 14, no. 4, 947-970

633 Karion, A., C. Sweeney, P. Tans, T. Newberger (2010), AirCore: An innovative atmospheric  
634 sampling system, *J. Atmos. Oceanic Technology* 27, 1839-1853. doi:  
635 10.1175/2010JTECHA1448.1





- 636 Lekner, J. (2019), Laminar viscous flow through pipes, related to cross-sectional area and  
637 perimeter length, *Am. J. Phys.* 87, 791, doi: 10.1119/1.5113573
- 638 Massman, W. (1998), A review of the molecular diffusivities of H<sub>2</sub>O, CO<sub>2</sub>, CH<sub>4</sub>, CO, O<sub>3</sub>, NH<sub>3</sub>,  
639 N<sub>2</sub>O, NO, and NO<sub>2</sub> in air, O<sub>2</sub> and N<sub>2</sub> near STP, *Atmos. Environm.* 32, 1111-1127
- 640 Moore, F., E. Ray, K. Rosenlof, J. Elkins, P. Tans, and C. Sweeney (2014), A cost effective trace  
641 gas measurement program for long term monitoring of the stratospheric circulation, *Bull. Amer.*  
642 *Meteo. Soc.*, 95, 147-155, doi: 10.1175/BAMS-D-12-00153.11G
- 643 O'Hanlon, J. (1980), *A user's guide to vacuum technology*, Wiley & Sons, New York, ISBN 0-  
644 471-01624-1
- 645 Press, W., S. Teukolski, W. Vetterling, and B. Flannery (1992), *Numerical Recipes in Fortran*,  
646 2<sup>nd</sup> Edition, Cambridge University Press, ISBN 0-521-43064-X
- 647 Sevast'yanov, R., and R. Chernyavskaya (1986), Virial coefficients of nitrogen, oxygen, and air  
648 at temperatures from 75 to 2500 K, *J. Engineer., Phys. and Thermophys.* 51, 851-854.
- 649 Swagelok (2020), *Valve Sizing Technical Bulletin*, downloaded September 2020 from  
650 [www.swagelok.com/en/toolbox/cv-calculator](http://www.swagelok.com/en/toolbox/cv-calculator)
- 651 Tans, P. (2009), System and method for providing vertical profile measurements of atmospheric  
652 gases. U.S. Patent 7,597,014 (6 Oct. 2009)
- 653 VIM3, International vocabulary of metrology – Basic and general concepts and associated terms,  
654 JCGM 200:2008, published by Bureau International de Poids et Mesures (BIPM).
- 655 Wagenhäuser, T., A. Engel, R. Sitals (2021), Testing the altitude attribution and vertical  
656 resolution of AirCore measurements with a new spiking method, *Atmos. Meas. Techn.* 14, 1-12,  
657 doi: 10.5194/amt-14-1-2021.
- 658
- 659
- 660